Supporting Information for

Spin-splitting and switchable half-metallicity in van der Waals multiferroic $CuBiP_2Se_6$/GdClBr heterojunction

Kai Zhang[1], Xiaocha Wang[1,*], Wenbo Mi[2]

[1]*Tianjin Key Laboratory of Film Electronic & Communicate Devices, School of Integrated Circuit Science and Engineering, Tianjin University of Technology, Tianjin 300384, China*

[2]*Tianjin Key Laboratory of Low Dimensional Materials Physics and Preparation Technology, School of Science, Tianjin University, Tianjin 300354, China*

[*]Author to whom all correspondence should be addressed.

E-mail: wangxc@email.tjut.edu.cn

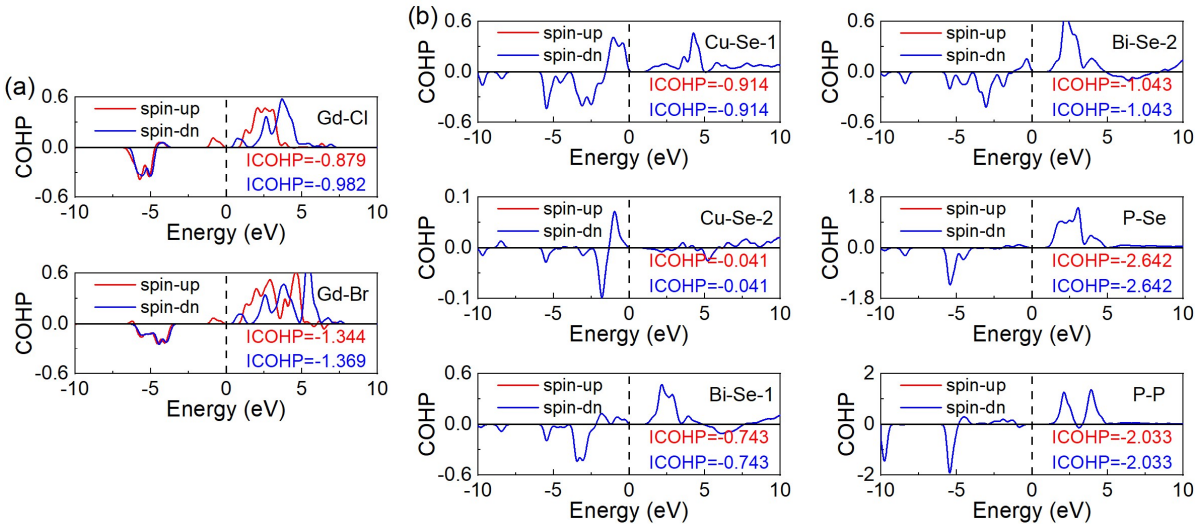

Fig. S1. The crystal orbital Hamilton population (COHP) of intra-layer interaction for (a) GdClBr monolayer, (b) $CuBiP_2Se_6$ monolayer.

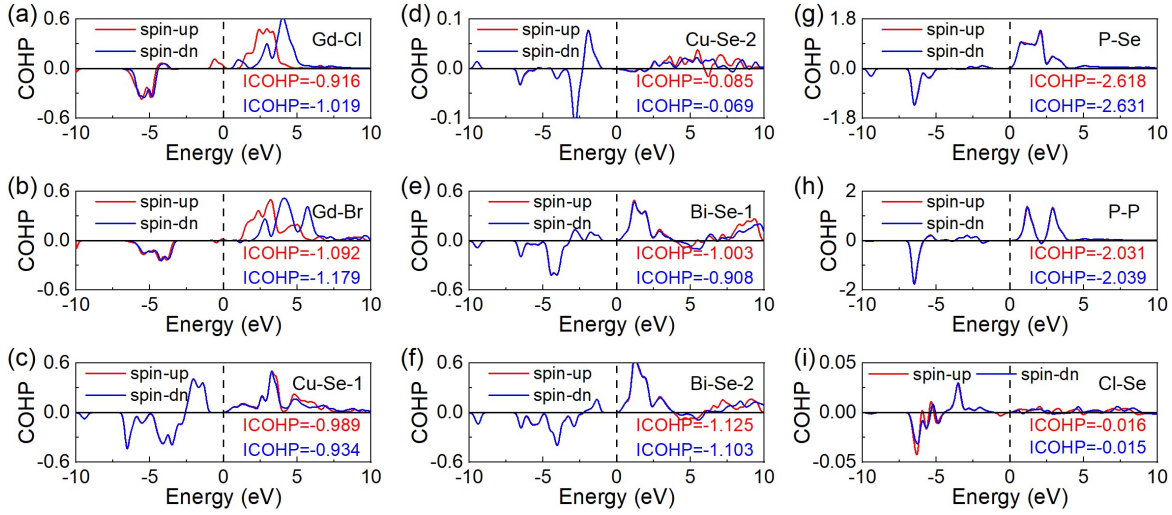

Fig. S2. The crystal orbital Hamilton population (COHP) of intra-layer interaction and interlayer interaction for GdClBr/$CuBiP_2Se_6$ of modle4.

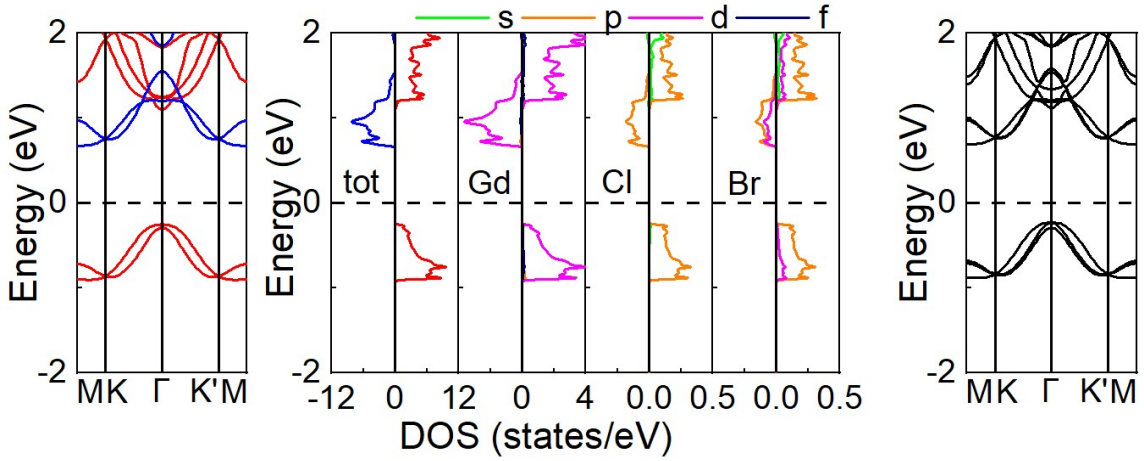

Fig. S3. The band structure, total and partial density of states of the supercell GdClBr by √3*√3*1 near Fermi energy level without/with SOC. The Fermi level is set at 0 eV.

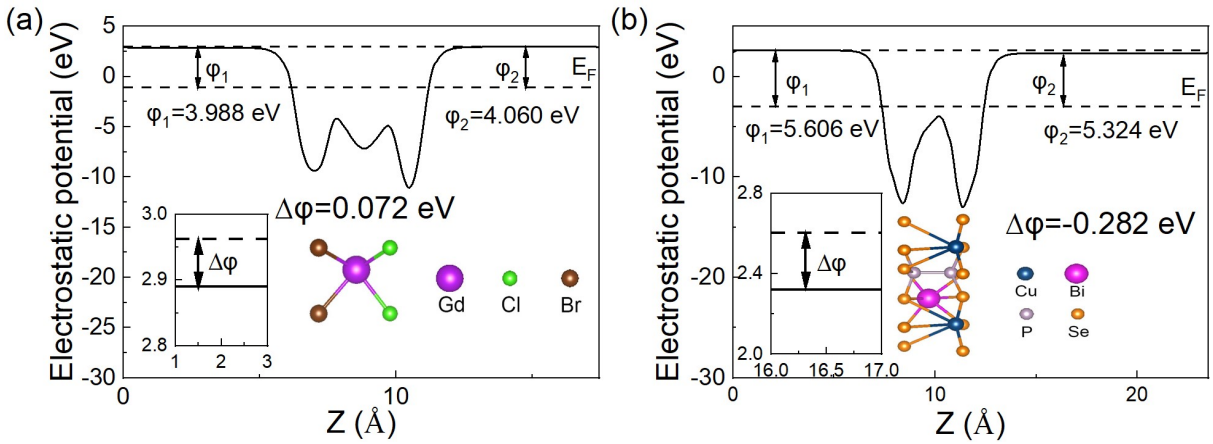

Fig. S4. The planar average of electrostatic potential along the z axis of (a) GdClBr and (b) $CuBiP_2Se_6$.

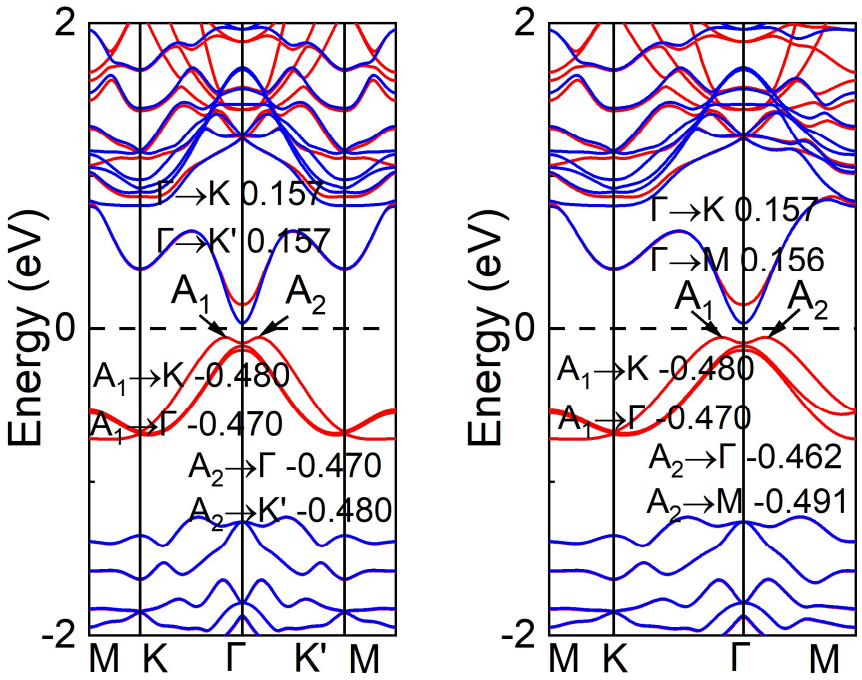

Fig. S5. The band structures of $GdClBr/CuBiP_2Se_6$ of modle4 are divided by MKΓK'M and MKΓM, which electron effective mass at CBM and VBM, along different paths of high symmetric point are marked in the band structures, respectively. (The hole effective mass values are positive)

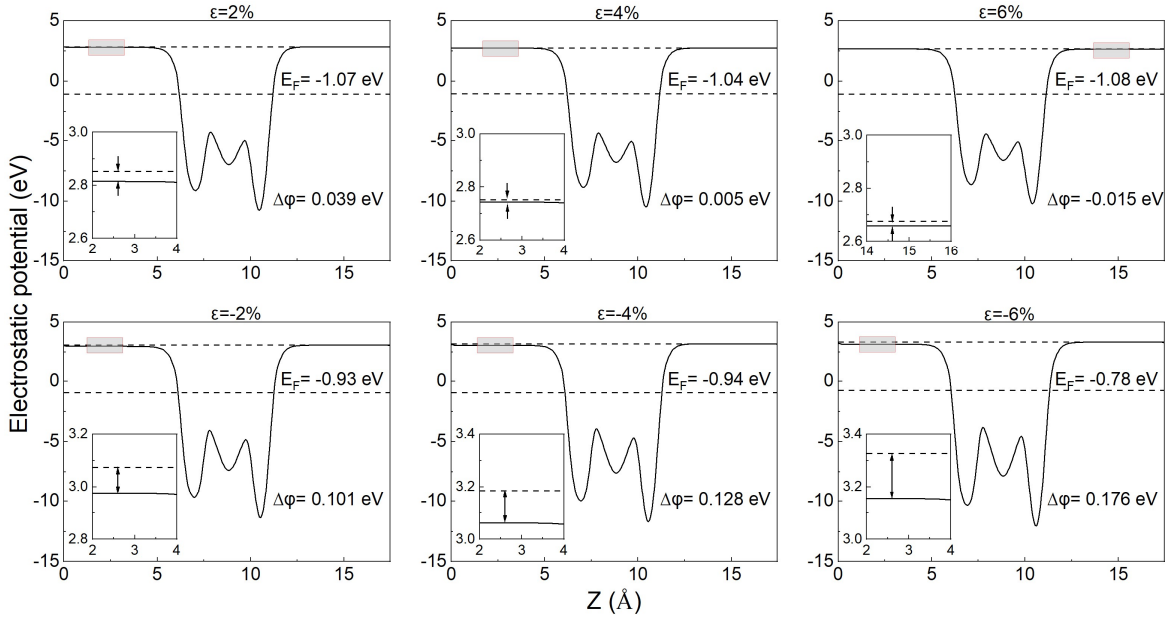

Fig. S6. The planar average of electrostatic potential along the z-axis of GdClBr at biaxial strain from -6% to 6%.

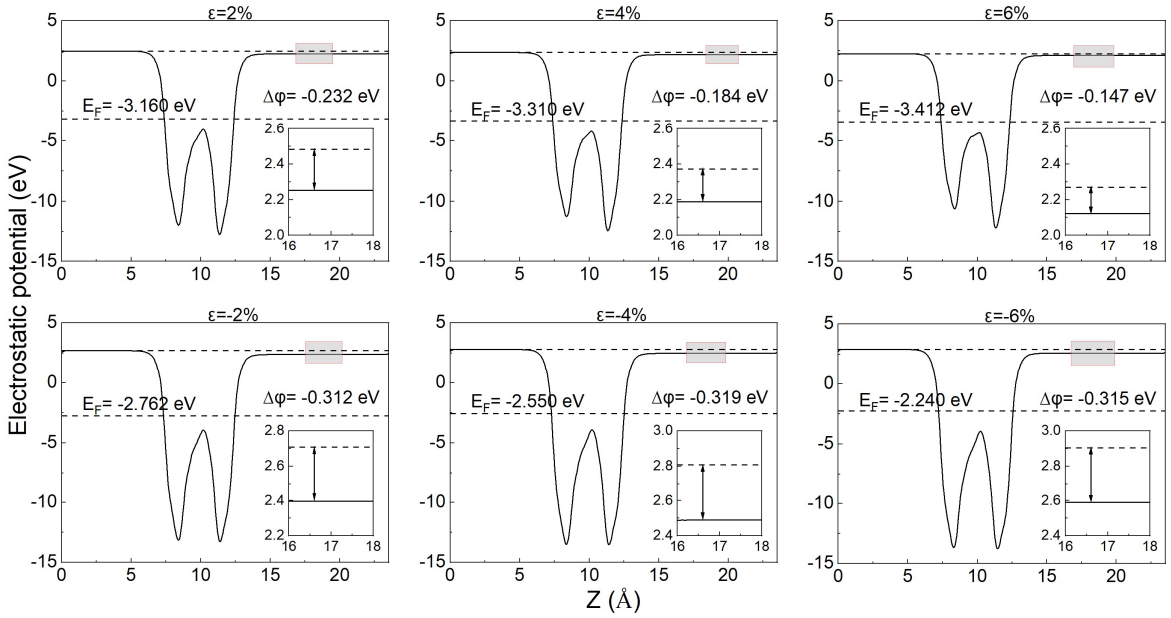

Fig. S7. The planar average of electrostatic potential along the z-axis of $CuBiP_2Se_6$ at biaxial strain from -6% to 6%.

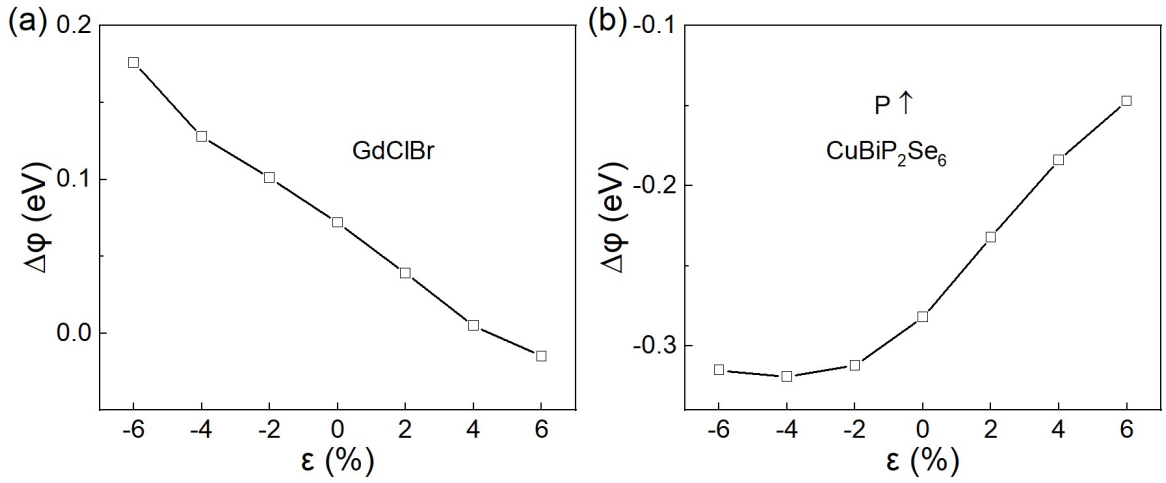

Fig. S8. Schematic diagram of the work function difference of (a) GdClBr and (b) $CuBiP_2Se_6$ at biaxial strain from -6% to 6%.

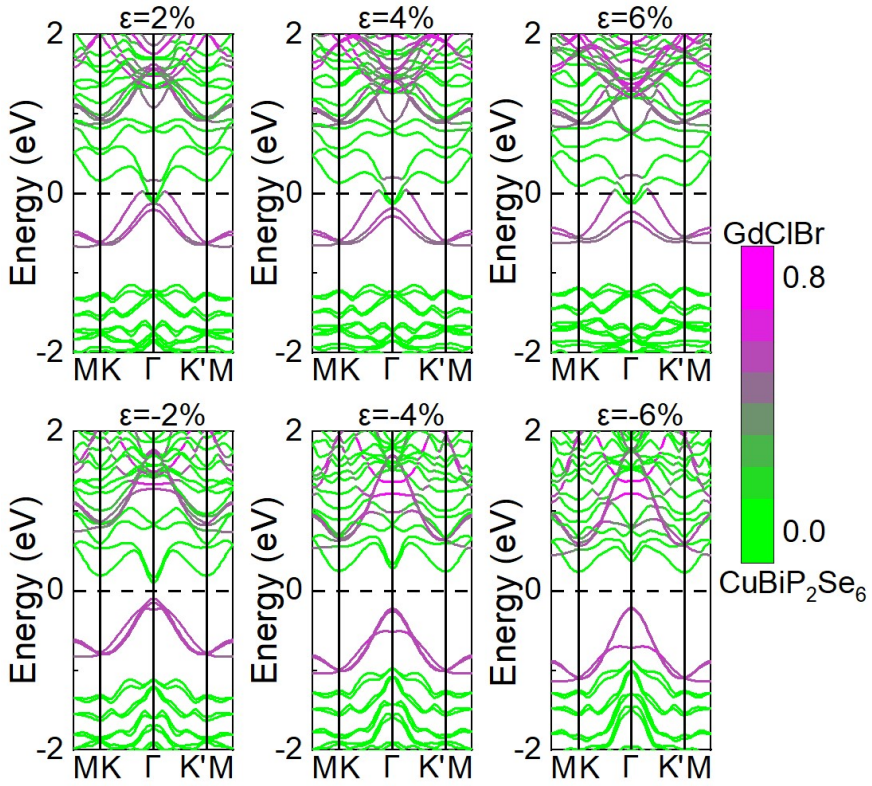

Fig. S9. The band structure of the model4 of GdClBr/$CuBiP_2Se_6$ near Fermi energy level at biaxial strain from -6% to 6% with SOC. The Fermi level is set at 0 eV.

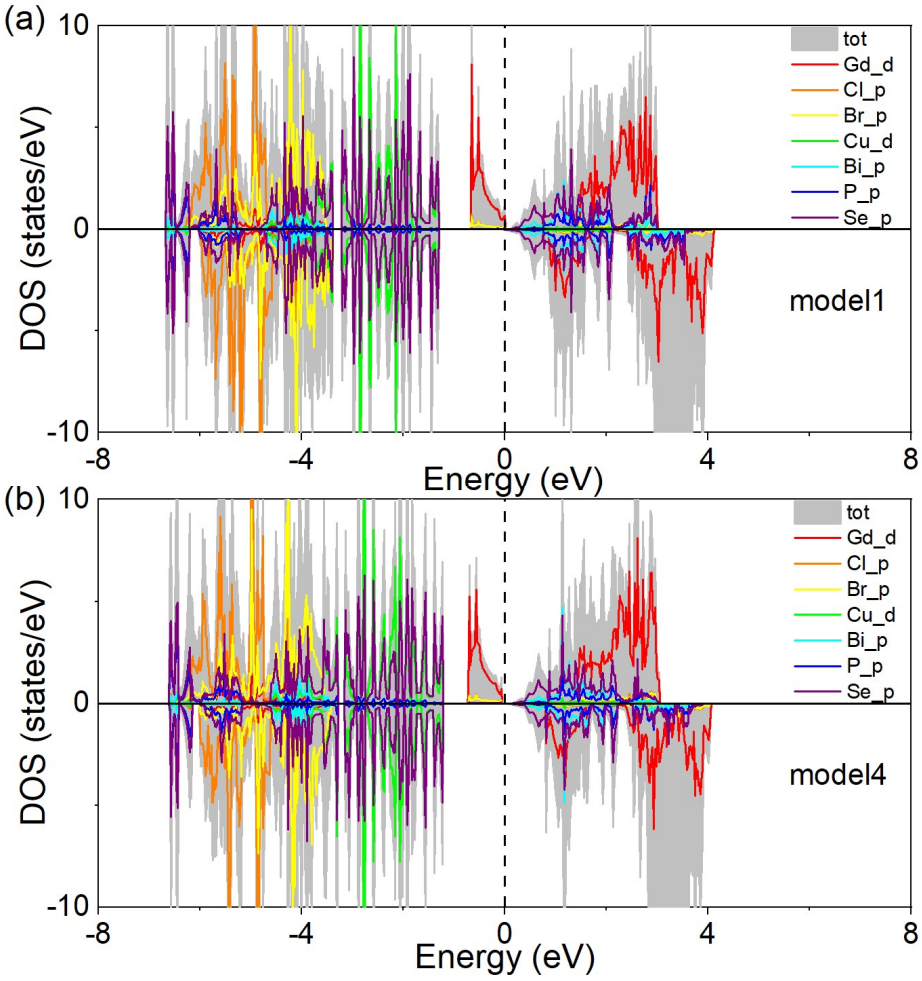

Fig. S10. Total and partial density of states of (a) model1 and (b) model4 of GdClBr/$CuBiP_2Se_6$ in an energy range from -8 eV to 8 eV.

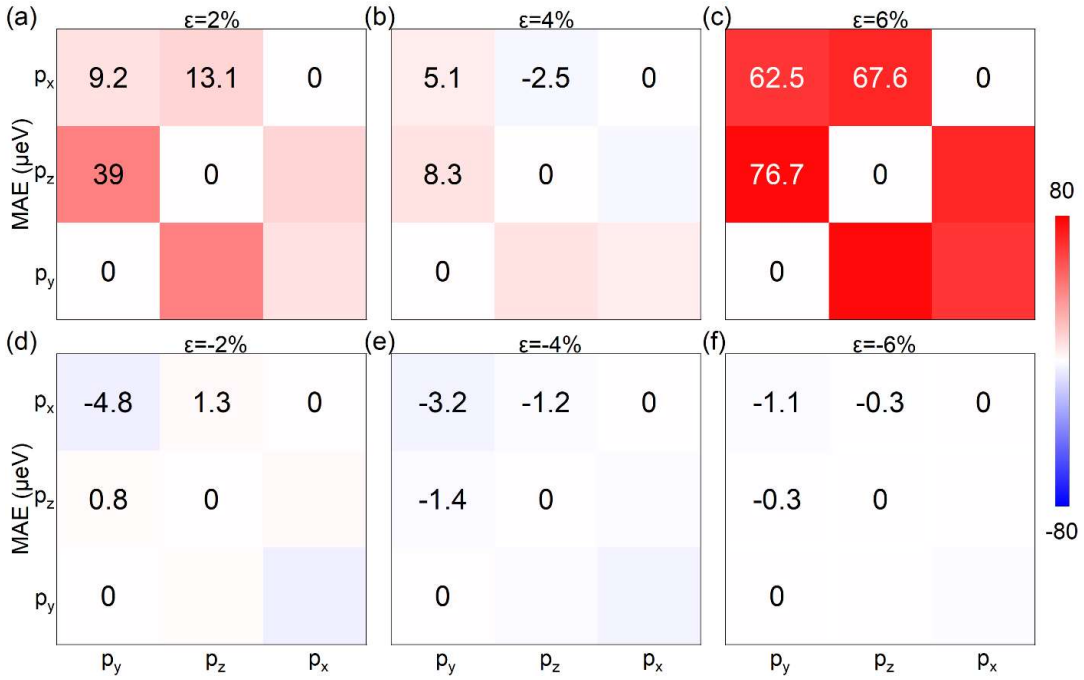

Fig. S11. Bi-p orbit-resolved MAE of the model4 of GdClBr/$CuBiP_2Se_6$ at a biaxial strain from (a) to (f) -6% to 6%.

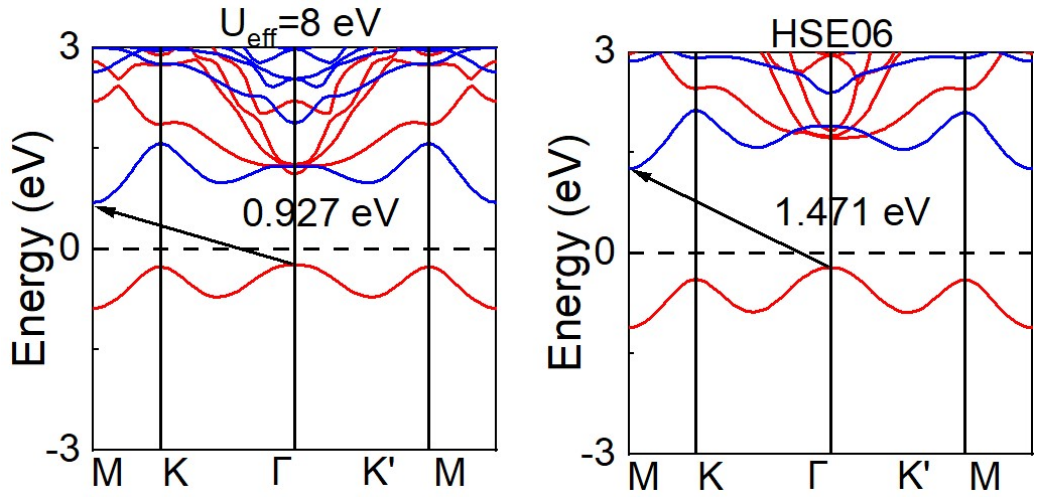

Fig. S12. The band structure of GdClBr near Fermi energy level without SOC by PBE+*U* and HSE06, respectively. The Fermi level is set at 0 eV.

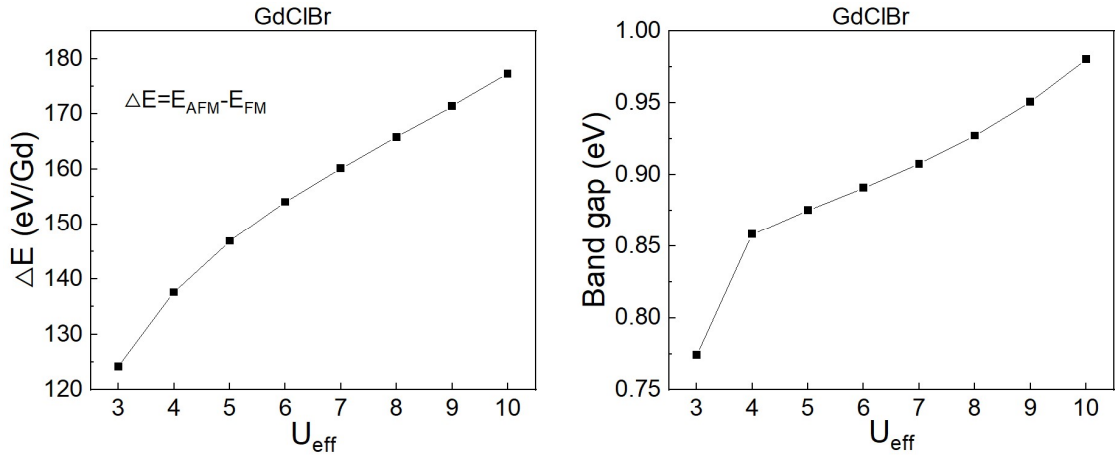

Fig. S13. Energy difference (ΔE) and band gap of GdClBr monolayer under different U_{eff}.

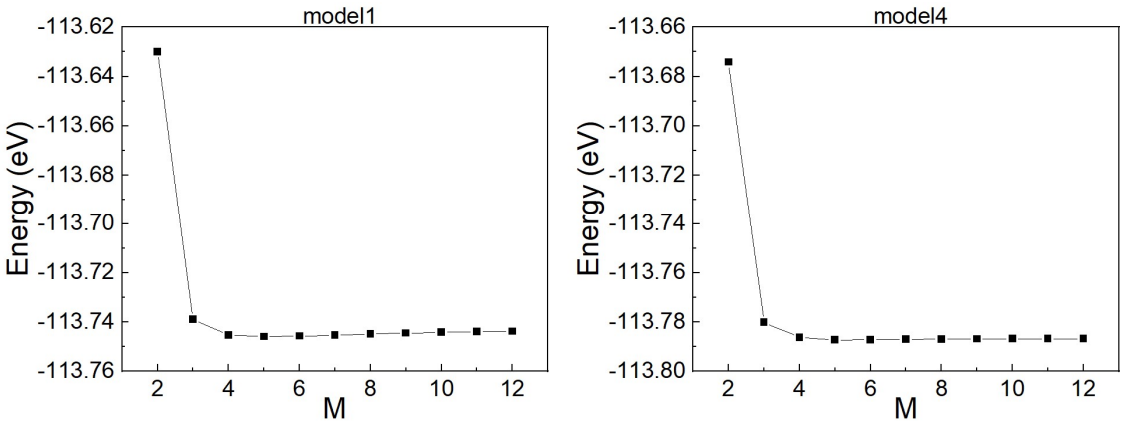

Fig. S14. Total energy of GdClBr/$CuBiP_2Se_6$ of model1 and model4 are calculated by using k-mesh of M×M×1.

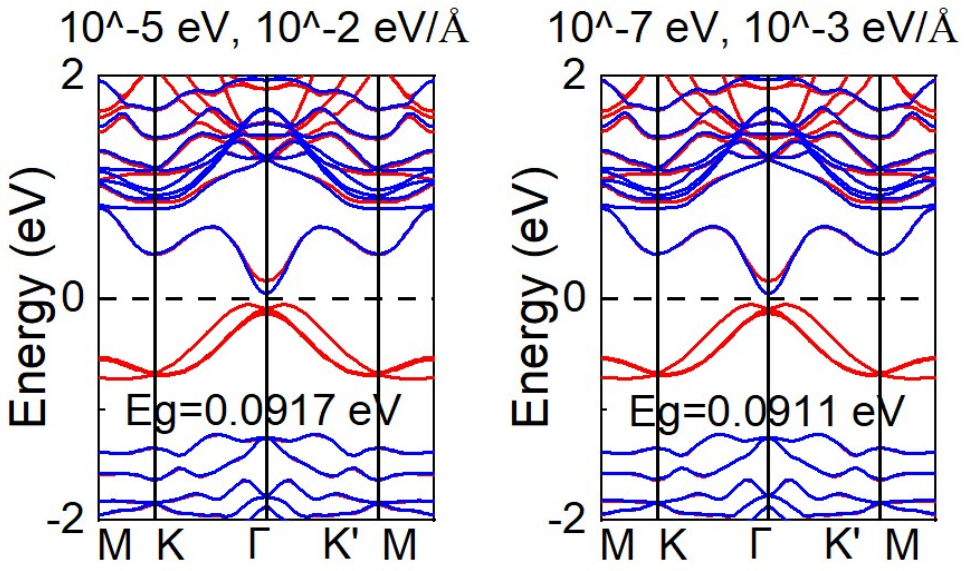

Fig. S15. The band structures of GdClBr/$CuBiP_2Se_6$ of modle4 are obtained by different energy and force convergence criteria on each atom. The Fermi level is set at 0 eV.

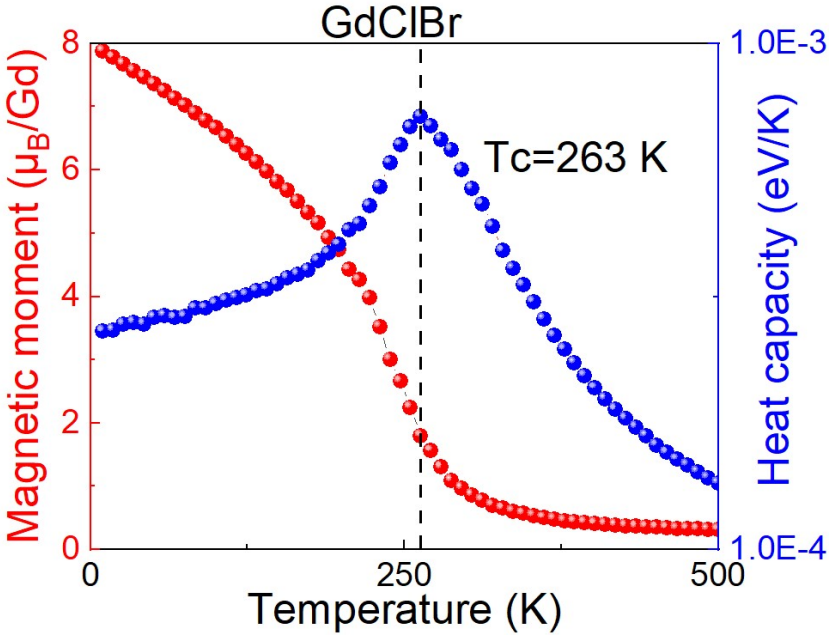

Fig. S16. The magnetic moment (red) and heat capacity (blue) as functions of temperature for GdClBr monolayer.

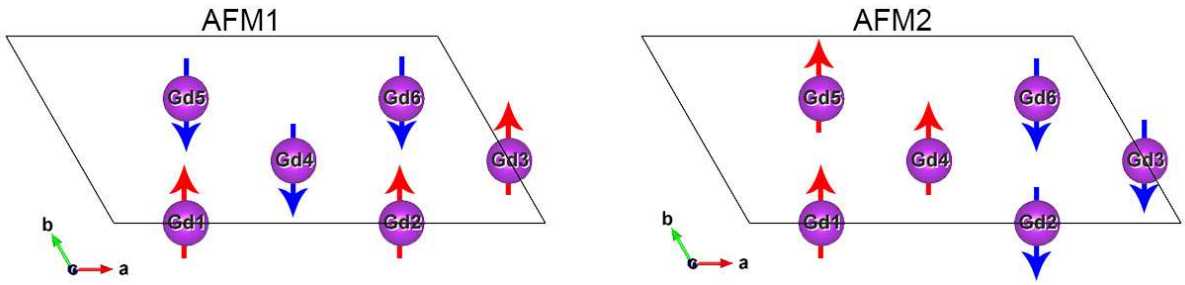

Fig. S17. The coordination environment of the Gd atom in the top of GdClBr/$CuBiP_2Se_6$ for two AFM configurations. The 2×1×1 supercell is marked by the solid lines. The red and blue arrows indicate spin-up and spin-down states, respectively.

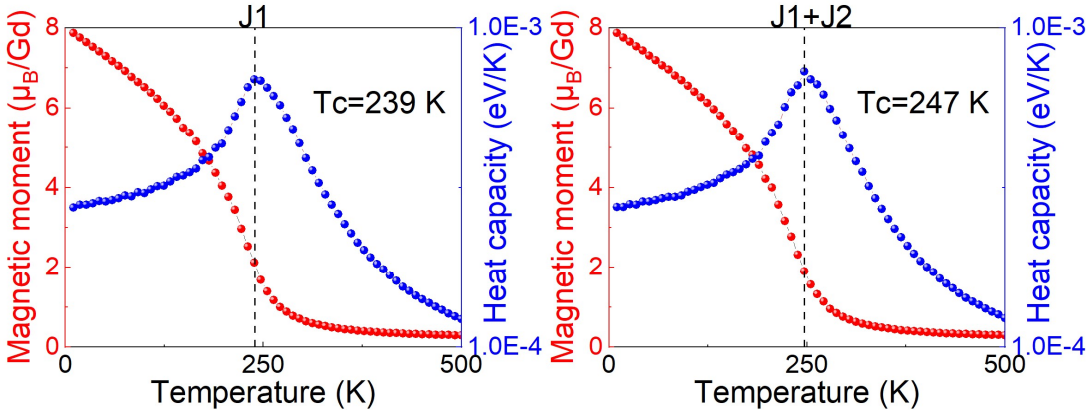

Fig. S18. The magnetic moment (red) and heat capacity (blue) as functions of temperature for model4 of GdClBr/$CuBiP_2Se_6$ by using methods of J_1 and methods of J_1+J_2, respectively.

Table. S1. Electron effective mass (m_n^*) and hole effective mass (m_p^*) along different paths of high symmetric point, average effective mass (m_d) of electron (hole) at CBM (VBM) for GdClBr/$CuBiP_2Se_6$ of modle4.

		Γ-K	Γ-K'(M)	A_1-K	A_1-Γ	A_2-Γ	A_2-K'(M)	m_d(Γ)	m_d(A_1)	m_d(A_2)
MKΓ	$m_n^*(m_p^*)$	0.157	0.157	0.480	0.470	0.470	0.480	0.157	0.475	0.475
K'M	$/m_0$									
MK	$m_n^*(m_p^*)$	0.157	0.156	0.480	0.470	0.462	0.491	0.156	0.475	0.476
ΓM	$/m_0$									

Table. S2. Energy difference (Δ*E*) of 2×1×1 supercell ferromagnetic configuration and 2×1×1 supercell antiferromagnetic configuration, exchange parameter (*J*), magnetic anisotropy energy (*MAE*), magnetic anisotropy energy parameter (*A*), the easy magnetization axis (EA) of GdClBr/$CuBiP_2Se_6$ and GdClBr monolayer.

	Δ*E* (meV)	*J* (meV)	*MAE* (μeV)	*A* (μeV)	EA
model1	922.62	2.403	594.4	12.383	PMA
model4	920.91	2.398	108.2	2.254	PMA
GdClBr	331.61	2.591	52.3	3.269	PMA

Table. S3. The work function of GdClBr (φ_{GdClBr}) and $CuBiP_2Se_6$ ($\varphi_{CuBiP2Se6}$) at the side near the interface, work function difference of GdClBr/$CuBiP_2Se_6$ at the interface at a biaxial strain from -6% to 6%.

	φ_{GdClBr} (eV)	$\varphi_{CuBiP2Se6}$ (eV)	$\Delta\varphi$ (eV)
ε = -6%	4.101	4.855	0.754
ε = -4%	4.116	5.066	0.950
ε = -2%	4.013	5.183	1.170
ε = 0%	4.060	5.324	1.264
ε = 2%	3.924	5.432	1.508
ε = 4%	3.795	5.447	1.652
ε = 6%	3.738	5.548	1.810

Table. S4. Energy difference (ΔE) of 2×1×1 supercell ferromagnetic configuration and 2×1×1 supercell antiferromagnetic configuration, exchange parameter (J), magnetic anisotropy energy (MAE), magnetic anisotropy energy parameter (A), the easy magnetization axis (EA) of GdClBr/$CuBiP_2Se_6$ at a biaxial strain from -6% to 6%.

	ΔE (meV)	J (meV)	MAE (μeV)	A (μeV)	EA
ε = 0%	920.91	2.398	108.2	2.254	PMA
ε = 2%	904.48	2.355	-228.6	-4.763	IMA
ε = 4%	888.21	2.313	-792.6	-16.513	IMA
ε = 6%	881.83	2.296	-856.9	-17.852	IMA
ε = -2%	941.02	2.451	475.1	9.898	PMA
ε = -4%	960.68	2.502	818.8	17.058	PMA
ε = -6%	975.8	2.541	1105.6	23.033	PMA

Table. S5. Total energy (E), band gap (E_g), magnetic anisotropy energy (MAE), energy difference (ΔE) of 2×1×1 supercell ferromagnetic configuration and 2×1×1 supercell antiferromagnetic configuration of GdClBr/$CuBiP_2Se_6$ of modle4 with different energy and force convergence criteria on each atom.

	E (eV)	E_g (eV)	MAE (μeV)	$\Delta E(E_{4FM}\text{-}E_{FM})$ (meV)
10^-5 eV, 10^-2 eV/Å	-113.78692	0.0917	108.2	920.91
10^-7 eV, 10^-3 eV/Å	-113.78702	0.0911	110.4	920.29

Table. S6. Energy difference (ΔE) of ferromagnetic configuration and antiferromagnetic configuration of GdClBr/$CuBiP_2Se_6$ for 2×1×1 supercell.

	$\Delta E(E_{AFM}\text{-}E_{FM})$ (meV)
AFM1	920.91
AFM2	623.61